Tectonophysics 680 (2016) 129–139

Contents lists available at ScienceDirect

Tectonophysics

journal homepage: www.elsevier.com/locate/tecto

Microstructural evolution and rheology of quartz in a mid-crustal shear zone

Jeffrey M. Rahl [a,*], Philip Skemer [b]

[a] Department of Geology, Washington and Lee University, Lexington, VA 24450, USA
[b] Department of Earth and Planetary Sciences, Washington University in St. Louis, Saint Louis, MO 63130, USA

ARTICLE INFO

Article history:
Received 28 June 2015
Received in revised form 27 April 2016
Accepted 10 May 2016
Available online 13 May 2016

Keywords:
Quartz
CPO
Mylonite
Deformation mechanisms
Recrystallization

ABSTRACT

We present microstructural and crystallographic preferred orientation (CPO) data on quartz deformed in the middle crust to explore the interaction and feedback between dynamic recrystallization, deformation processes, and CPO evolution. The sample investigated here is a moderately deformed quartz-rich mylonite from the Blue Ridge in Virginia. We have created high-resolution crystallographic orientation maps using electron backscatter diffraction (EBSD) of 51 isolated quartz porphyroclasts with recrystallized grain fractions ranging from 10 to 100%. Recrystallized grains are internally undeformed and display crystallographic orientations dispersed around the orientation of the associated parent porphyroclast. We document a systematic decrease in fabric intensity with recrystallization, suggesting that progressive deformation of the recrystallized domains involves processes that can weaken a pre-existing CPO. Relationships between recrystallization fraction and shear strain suggest that complete microstructural re-equilibration requires strains in excess of $\gamma = 5$. Variation in the degree of recrystallization implies that strain was accumulated heterogeneously, and that a steady-state microstructure and rheology were not achieved.

1. Introduction

Quartz exerts an important control on the rheology of the continental crust, and under certain conditions it may represent the strongest mechanical element of the lithosphere (e.g., Kohlstedt et al., 1995; Bürgmann and Dresen, 2008). At conditions typical of the middle to lower crust, quartz deformation generally proceeds by dislocation creep processes (Hirth and Tullis, 1992). As dislocations accumulate in a crystal, the associated strain energy promotes dynamic recrystallization, in which the migration of grain boundaries and/or the migration of dislocations to sub-grain boundaries creates crystals with a lower free dislocation density (e.g., Urai et al., 1986). Likewise, during dislocation creep, a crystallographic preferred orientation (CPO) is developed. The preferential alignment of grains with particular crystallographic orientation may introduce anisotropy in both seismological and rheological properties (e.g., Kocks et al., 2000). Feedbacks between deformation processes, dynamic recrystallization, and CPO development are known to have a profound effect on the rheology and anisotropy of many important minerals in Earth, including olivine (Warren and Hirth, 2006; Précigout et al., 2007; Knoll et al., 2009; Kaczmarek and Tommasi, 2011; Skemer et al., 2013), pyroxene (Raimbourg et al., 2008; Skemer and Karato, 2008), and feldspar (Jiang et al., 2000; Mehl and Hirth, 2008).

Although the effects of dynamic recrystallization on the rheology of quartz-rich shear zones are likely to be profound, significant questions persist. Grain-size reduction due to dynamic recrystallization may induce strain-weakening through transitions to grain-size sensitive deformation mechanisms (Rutter and Brodie, 1988; Kilian et al., 2011a; Linckens et al., 2011), but due to uncertainties with empirical flow laws the deformation conditions where this occurs are poorly known (Behr and Platt, 2011). CPO is commonly used to draw inferences about deformation, including deformation temperature (Schmid and Casey, 1986; Stipp et al., 2002b; Toy et al., 2008; Law, 2014), shear sense (Kilian et al., 2011b; Toy et al., 2012), or strain (Carreras and García Celma, 1982). However, experimental data relating dynamic recrystallization to strain and CPO evolution are limited (Heilbronner and Tullis, 2002; Heilbronner and Tullis, 2006; Muto et al., 2011), and it is unclear how quartz CPO evolves over a wide range of deformation conditions and deformation mechanisms.

In this contribution, we use a quartz-rich mid-crustal mylonite as a natural laboratory to investigate the coupled processes of dynamic recrystallization, grain-size reduction, and the evolution of CPO. The sample targeted in this study is from the Rockfish Valley Deformation Zone in the Blue Ridge province of Virginia, a 1–3 km thick zone of mylonitic deformation representative of mid-crustal shear zones (Bailey and Simpson, 1993). Isolated quartz porphyroclasts within the sample

* Corresponding author.
E-mail address: rahlj@wlu.edu (J.M. Rahl).

http://dx.doi.org/10.1016/j.tecto.2016.05.022
0040-1951/

preserve variable degrees of recrystallization, from less than 20% to fully recrystallized. This microstructural variation provides a valuable opportunity to assess quantitatively the impacts of strain and recrystallization on CPO development in quartz.

2. Sample material

2.1. Geologic setting

The studied sample was collected from the Rockfish Valley Deformation Zone (RVDZ), a NE–SW striking and moderately SE-dipping zone of anastomosing protomylonites, mylonites, and local ultramylonites (Fig. 1). The RFDZ developed within the crystalline basement of the Grenville-aged Blue Ridge province (Bartholomew et al., 1981; Sinha and Bartholomew, 1984; Aleinikoff et al., 2000). The regionally-significant structure has been traced for over 120 km along strike in central Virginia (Bailey and Simpson, 1993) and may connect with the Fries fault zone to the south (Bartholomew et al., 1981). Although the total magnitude of displacement across the RVDZ is unknown, empirical scaling relationships indicate that the 3 km or greater thickness of the RVDZ corresponds with a conservative displacement estimate of 7 km (Hull, 1988). The time of deformation of the RVDZ has been debated (cf., Bartholomew et al., 1991; Evans, 1991; Bailey and Simpson, 1993), but recent white-mica argon work suggests thrust-related cooling between 345 and 320 Ma (Jenkins et al., 2012).

Both macro- and micro-scale shear sense indicators consistently suggest top NW-thrust sense motion parallel to a prominent down-dip mineral elongation lineation within the foliation plane (Figs. 1 and 2). Previous microstructural studies document ubiquitous evidence for non-coaxial greenschist facies deformation (Campbell and Anderson, 1992; Bailey and Simpson, 1993; Bailey et al., 1994; Spencer, 1995). Quartz appears either as porphyroclasts or elongate ribbons, typically exhibiting a sweeping undulose extinction or recrystallization. Fine-grained quartz often displays a shape-preferred orientation aligned obliquely to the dominant foliation. Abundant and generally perthitic feldspar porphyroclasts are commonly fractured and extended and only rarely show evidence of internal deformation (Bailey et al., 1994). The combination of fractured feldspar grains and plastically deformed quartz suggests deformation temperatures within the shear zone were likely below 450 °C (e.g., Stipp et al., 2002b).

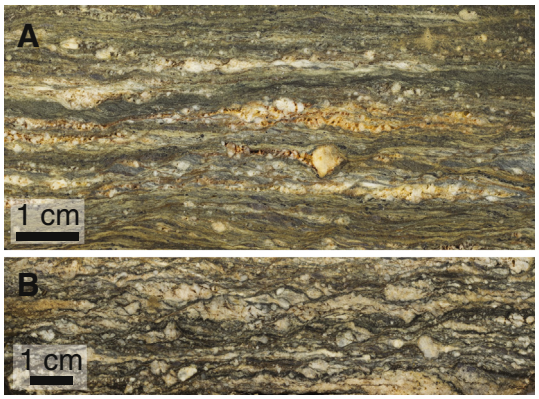

Fig. 2. A, B) Polished slabs of rock from the studied locality, illustrating top-NW kinematic indicators, including asymmetric feldspar porphyroclasts and extensional shear-bands. The sense of shear in these images is sinistral.

2.2. Sample description

We focus on a porphyroclastic mylonite collected from the RFDZ near the James River Gap in central VA. Although perthitic feldspars are common throughout the RFDZ, porphyroclasts in the studied sample are almost exclusively quartz (Fig. 3). These occur either as porphyroclasts with aspect ratios up to 3:1 with long axes up to about 1 mm in length, or as elongate ribbons with aspect ratios reaching up to 10:1. Both the more equant porphyroclasts and the ribbons show undulose extinction and variable degrees of subgrain development and recrystallization. The porphyroclasts are often fish-shaped and aligned obliquely to the dominant foliation, consistent with top-NW motion (Passchier and Trouw, 2005). Quartz shows a bimodal grain-size distribution, with smaller grains interpreted as the product of dynamic recrystallization. Recrystallization is mainly developed along the margins of the quartz porphryoclasts, giving a "core-and-mantle"

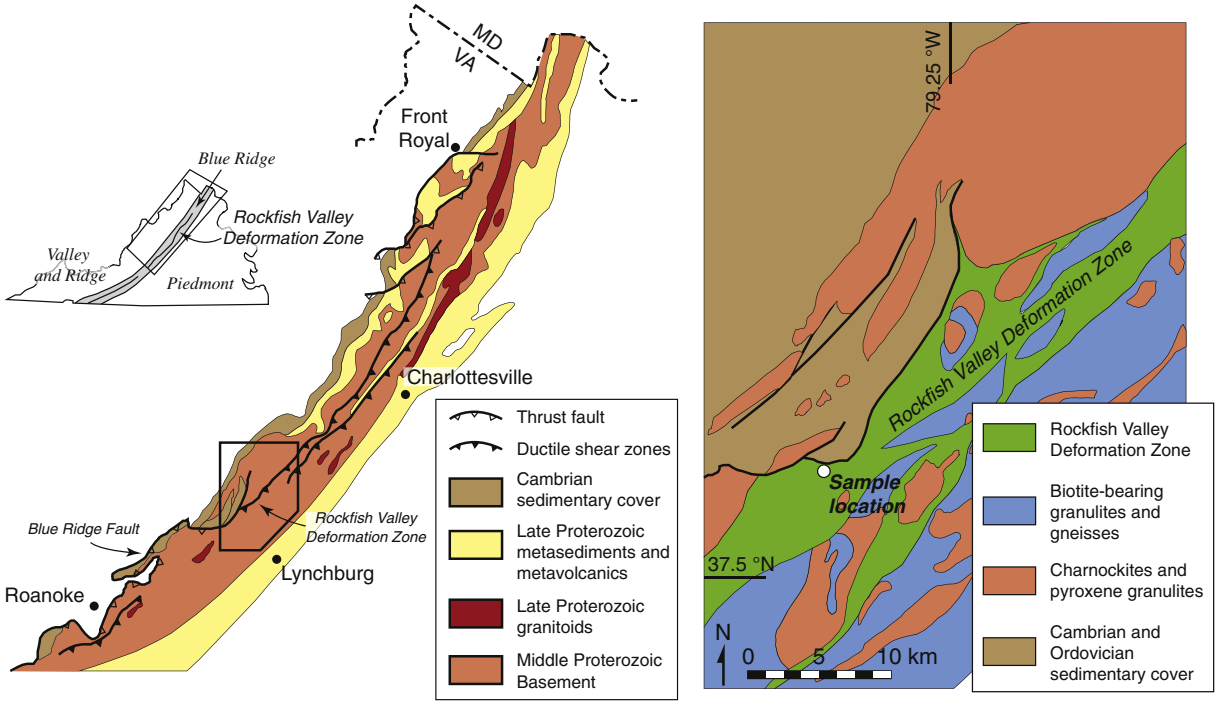

Fig. 1. Left: Generalized geologic map of the Blue Ridge, after Bailey and Simpson (1993); right: simplified geologic map of the study area, after Rader and Evans (1993).

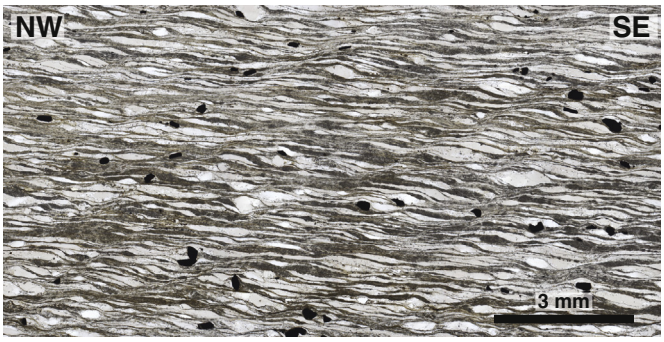

Fig. 3. Photomicrograph showing large-scale texture of the studied sample. Extensional shear bands (i.e., C′-type shear band cleavage) cut through the sample, from upper right to lower left. The large quartz porphyroclasts and ribbons often display a fish-like shape with their long dimensions oriented from lower right to upper left. The sample has a sinistral shear sense (top-NW).

structure (White, 1976) typical of recrystallization by subgrain rotation (Hirth and Tullis, 1992; Stipp et al., 2002a). Recrystallization is better developed in the ribbons, which commonly are completely recrystallized. The neoblasts appear as equant polygons with smooth and straight grain boundaries. The quartz microlithons are surrounded by a matrix of white mica, quartz, chlorite, stilpnomelane, titanite, and ilmenite. In places, porphyroclasts are mantled by fibrous strain shadows composed of quartz, white mica, and minor epidote (Fig. 4). Well-developed extensional shear bands cut obliquely through the sample, offsetting and further elongating the quartz microlithons (Fig. 3).

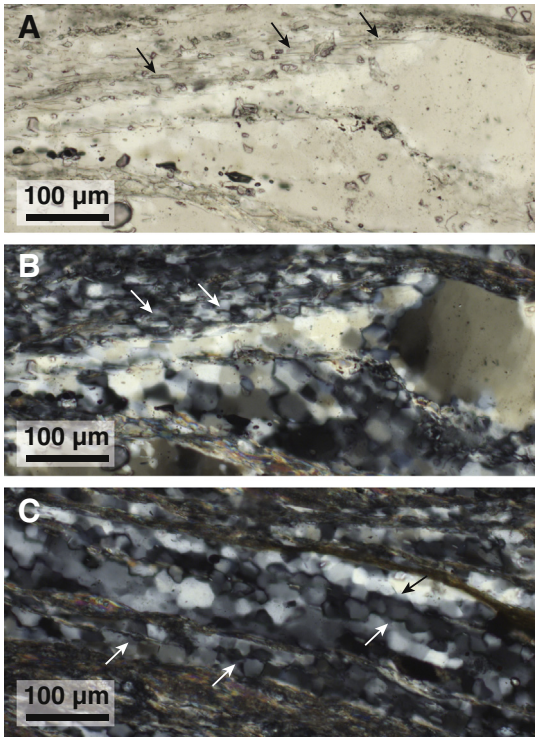

Fig. 4. Photomicrographs in of recrystallized porphyroclasts with adjacent strain fringes of quartz, white mica, and minor epidote, in plane cross-polarized light (A, B). Arrows in A and B identify thin grains of white mica oriented parallel to foliation. C. Cross-polarized photomicrograph of highly recrystallized porphyroclast; arrows highlight areas where straight grain boundaries span multiple grains, sometimes where secondary phases are aligned parallel to the length of the porphyroclast.

3. Methods

3.1. Microstructural data acquisition

We employed optical and electron microscopy and electron backscatter diffraction (EBSD) to characterize the crystallographic orientations and other deformation microstructures of quartz. Microstructural analysis was performed on a petrographic thin section oriented parallel to the macroscopic lineation and perpendicular to foliation. For EBSD analysis, the thin-section was mechanically polished using diamond abrasives and then subjected to a final chemical–mechanical polishing step using a 0.04 μm colloidal silica slurry. The sample was analyzed on a Zeiss EVO MA 15, Scanning Electron Microscope (SEM) at Washington and Lee University using an Oxford Instruments EBSD detector and Aztec software. Operating conditions were an accelerating voltage of 25 kV, a probe current of 20–25 nA, and a working distance between 15 and 25 mm. The sample was not coated, so to prevent charging the SEM was operated in low-vacuum mode at a pressure of 20–30 Pa.

Two sampling strategies were employed. First, to assess the crystallographic fabric preserved in the porphyroclasts, the unrecrystallized interiors of individual porphyroclasts were visually identified in the SEM and then analyzed for crystallographic orientation (one analysis per porphyroclast). A total of 472 porphyroclasts were measured in this manner. Second, to document the effects of recrystallization on quartz CPO, detailed mapping was performed on 51 individual porphyroclasts that exhibited a wide range of degree of recrystallization. For these porphyroclasts, an analysis was performed on a 2-dimensional grid with a step size of 1.5 or 2 μm.

3.2. EBSD data processing

The EBSD data were processed and analyzed using the MTEX toolbox for Matlab (Hielscher and Schaeben, 2008). MTEX employs a Voroni decomposition approach to reconstruct grains and grain-boundaries from raw EBSD data. Spatially adjacent observations with similar crystallographic orientations less than a 10° misorientation were placed into discrete cells (grains) separated by boundaries (Lloyd et al., 1997). Individual non-indexed points and small groups of points are assigned to adjacent grains; clusters of 8 or more adjacent non-indexed points are preserved as non-quartz grains. We also calculated subgrain boundaries, with misorientations between 2 and 5° or 5–10°.

Grain size is calculated as the diameter of a circle with an area equal to the measured domain; stereological effects are not considered. For the purpose of objectively identifying and isolating crystallographic data from the maps, we define two populations of grains: 1) “porphyroclasts,” defined to be grains with a diameter that is at least 4 times the median grain diameter within a given map and interpreted as unrecrystallized relicts, and 2) “neoblasts,” grains with smaller grain diameters that we infer to have formed by recrystallization. Our inspection of the resulting grain classifications indicates this definition works well; the identified porphyroclasts are larger, longer, and more internally distorted than the grains classified as neoblasts. We experimented with other definitions, using different thresholds (e.g., 6 times the median grain diameter) or properties (e.g., based on grain area), but these yield qualitatively similar results. The observed area of the neoblast and relict porphyroclast grains were used to determine the degree of recrystallization in each mapped microlithon.

The strength of the CPO for each region was assessed using the M-index (Skemer et al., 2005). The microlithons have an average of 290 grains, sufficient for robust quantitative determination of CPO intensity. For a few small or minimally recrystallized microlithons, the total number of grains present is less than the 150 grains required for robust M-index determination. In these cases (<10), the M-index provides an upper bound on CPO strength (Skemer et al., 2005).

For all mapped grains, we calculate the maximum internal misorientation (MIM) angle relative to the grain's mean orientation. The MIM provides information about the internal deformation of individual grains and is a proxy for dislocation density (Wheeler et al., 2012). Grains that are distorted internally by free dislocations or subgrain boundaries are expected to exhibit larger internal misorientation angles than those that are relatively undistorted by dislocation microstructures. To prevent outlier measurements from creating upwardly-biased estimates, we adopt as the maximum internal misorientation angle the 95th percentile value within each grain.

4. Results

4.1. CPO

Crystallographic orientations were measured from the unrecrystallized interiors of 472 porphyroclasts visually identified and selected from throughout the sample. The resulting quartz c-axis fabric (Fig. 5) shows an asymmetric type I cross-girdle (Lister, 1977). The observed CPO, with well-developed small circles around the Z direction, indicates a significant component of coaxial deformation. Quartz <a>-axes are inclined at low angle to the foliation plane, with a dominant maxima consistent with top-NW motion. The porphyroclast distribution compiled from the detailed microlithon mapping yields a similar but less well-defined CPO (created using just the mean orientation for each grain). Both datasets show a clear girdle, but the manually-identified porphyroclast dataset reveals more structure, including cross-girdles opening around the sample Z direction and a sense of asymmetry. We attribute the difference between these pole figures to the lower number of observations included within the map-based dataset (number of grains = 266). Furthermore, many of these observations are not truly independent, given that multiple porphyroclasts with similar orientations were typically identified in each of the 51 microlithon domains mapped at high resolution. The neoblast dataset, compiled from all the detailed maps, exhibits a CPO closely related to that of the parent porphyroclasts (Fig. 5), though weaker and more diffuse.

4.2. Recrystallization fraction and CPO intensity

The results from the individually scanned microlithons quantify the variable degree of recrystallization in microlithons, ranging from 10% to fully recrystallized (Figs. 6 and 7). We also observe a strong and monotonic relationship between the degree of recrystallization and the intensity of the microlithon's CPO (Fig. 7). Small degrees of recrystallization are associated with greater CPO intensity, approaching the single crystal

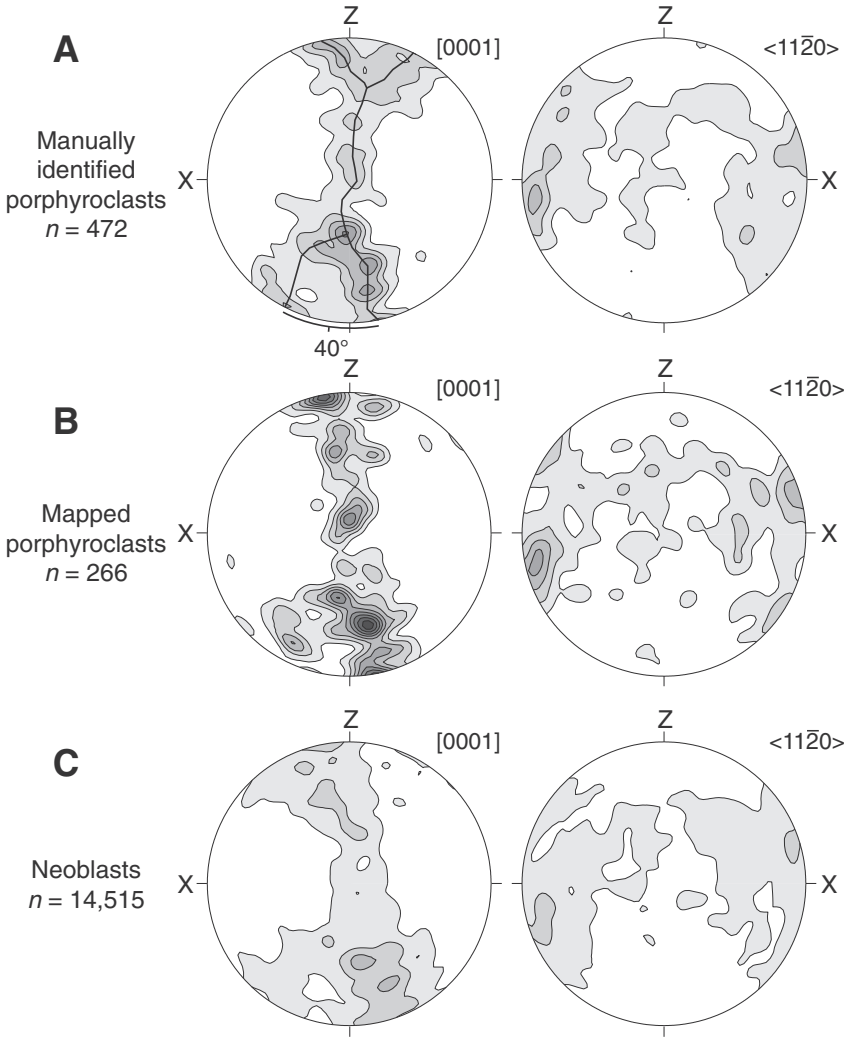

Fig. 5. Lower hemisphere pole figures of quartz crystallographic axes, based on one point per grain. Projection plane contains the macroscopic lineation direction (oriented horizontally) and the pole to the foliation plane (oriented vertically). Contours are at intervals of times mean uniform density, with shading saturated at 9 times uniform density. The quartz porphyroclasts were both manually identified from throughout the sample (upper diagram) or from detailed mapping of selected microlithons (middle diagram). The neoblast distribution (lower diagram) appears as a weaker and more diffuse version of that for the parent porphyroclasts.

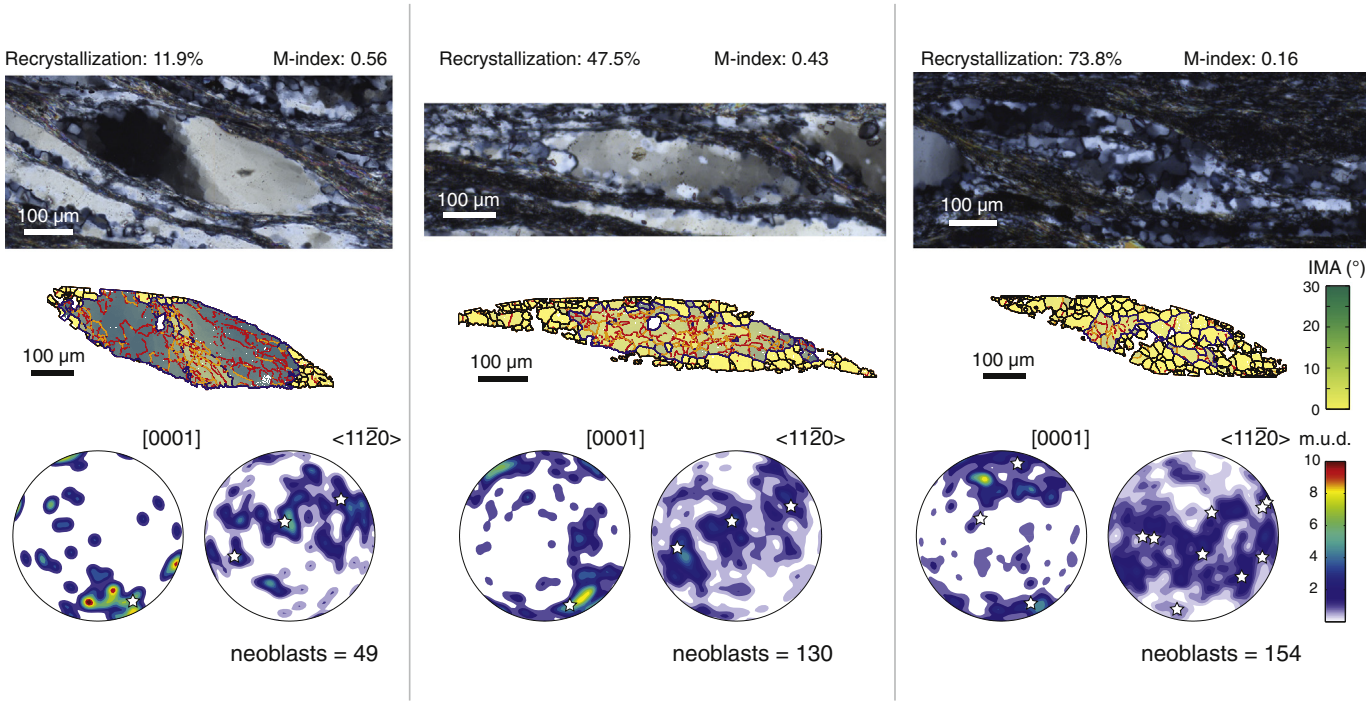

Fig. 6. Representative examples of quartz microlithons mapped by EBSD, displaying from left to right a range of crystallization fraction. *Upper panels*: cross-polarized light microscopic images. *Middle panels*: EBSD maps of the microlithons. Grain boundaries (>10° misorientation) for the neoblasts are shown in black; the porphyroclasts are highlighted with a thicker blue line. Subgrain boundaries are highlighted for misorientations of >2° (red lines) and >5° (orange lines). Individual pixels are colored with their internal misorientation angle relative to the mean orientation of their grain. White pixels correspond to unindexed points. *Lower panels*: Pole figures of the quartz c[0001] and a <11–20> crystallographic axes within each microlithon. The stars represent the porphyroclasts; the individual grains are circles colored based on their maximum internal misorientation angle. (For interpretation of the references to color in this figure legend, the reader is referred to the web version of this article.)

intensity from which the neoblasts are originally derived; higher degrees of recrystallization are associated with weaker CPOs. To recast these results as a function of shear strain, we compiled results from laboratory experiments on quartz deformation. Heilbronner and Tullis (2006) and Muto et al. (2011) both document a systematic relationship between recrystallization percentage and strain. Lacking a more sophisticated model, we assume the relationship between strain and recrystallization fraction is linear. We use the best-fit line through the experimental data to define a relationship between shear strain and the fraction of recrystallization in quartz. These results suggest that the porphyroclasts studied here experienced shear strains ranging from $\gamma = 1$–6.

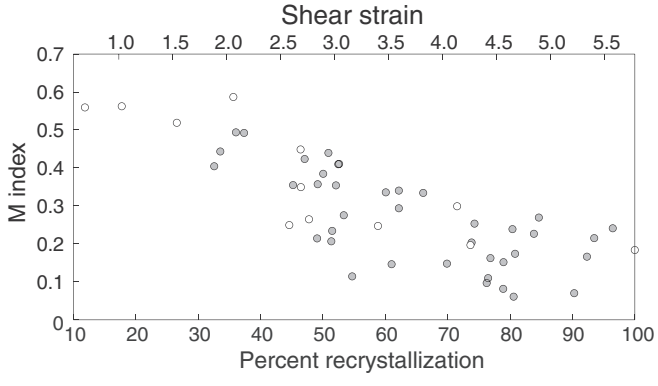

Fig. 7. Plot of fabric intensity, as measured by the M-index (Skemer et al., 2005) versus recrystallization percent for individual quartz microlithons. Microlithons with fewer than 150 grains are colored in white; for these samples, the M-index is best considered as an upper limit of fabric intensity. Shear strain values (shown on the upper x-axis) were calculated from linear regression of experimental data on recrystallization percentage and shear strain presented by Heilbronner and Tullis (2006) and Muto et al. (2011).

4.3. Maximum internal misorientation

The distributions of MIM angles are substantially different for the porphyroclast and neoblast datasets (Fig. 8). The porphyroclasts show comparatively large MIM angles, with most greater than 5° and some as large as 30°. In contrast, MIM within the neoblasts are very small, and nearly 90% of the neoblasts have MIM < 1°. Although EBSD measurements have a nominal absolute error of ~1° (e.g., Randle and Engler, 2000), this value does not represent the precision of repeated measurements within a single grain, which is much smaller. Moreover, the effect of measurement error would be to increase MIM angle by dispersing individual measurements within a grain by up to 1°, suggesting that the low observed MIM angles are robust.

We observe a strong non-linear relationship between the MIM angle and grain diameter (Fig. 9); larger grains are associated with greater angles. Clear differences exist between the porphyroclast and neoblast populations. By our definition the porphyroclasts must have greater

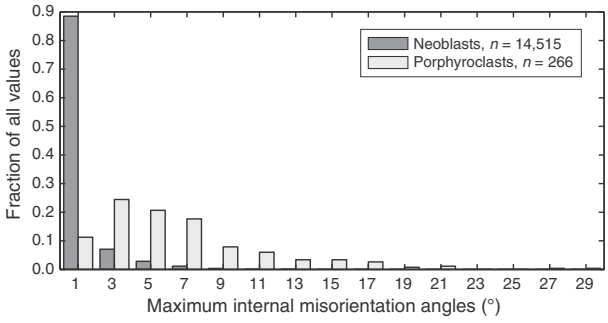

Fig. 8. Histogram of maximum internal misorientations for the quartz porphyroclasts (light gray) and neoblasts (dark gray). Heights are plotted as a fraction of all values. Data are grouped within 2° bins (i.e., 0–2°, 2–4°, etc.).

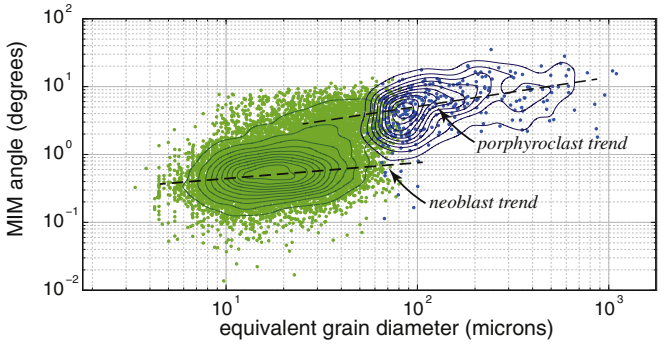

Fig. 9. Maximum internal misorientation angles as a function of equivalent grain diameter for the porphyroclasts (blue) and neoblasts (green). The colored lines show contours of data density for each dataset determined by through 2-dimensional kernel density estimation (Botev et al., 2010). The black dashed lines schematically illustrate the trends followed by the porphyroclast and neoblast datasets. (For interpretation of the references to color in this figure legend, the reader is referred to the web version of this article.)

grain diameters than the neoblasts, but they also exhibit significantly larger maximum misorientation angles. Given the large number of data, we employed a kernel smoothing approach to create relative frequency distributions to aid in data visualization. In the kernel density approach, the data density at a given point is smoothed using an averaging window (or "kernel") with a prescribed shape and width. We generated 2D kernel density estimate (KDE) plots in Matlab using an algorithm developed by Botev et al. (2010) that uses a Gaussian kernel with a size optimally determined based upon data density. To account for the non-linear relationship between internal misorientation angle and grain diameter, we first performed a log transform on the data. The KDE analysis generates a surface in grain diameter-maximum internal misorientation angle space in which greater heights correspond to higher data density. Contour plots of the surfaces for the neoblast and porphyroclast datasets clarify the data distribution (Fig. 9). The porphyroclast data define a simple trend with larger grains associated with higher MIM angles. In contrast, the bulk of the neoblast data show low maximum internal misorientation angles that increase more slowly as a function of grain size. A subset of the neoblast data appears as a shoulder on the main mass of data, corresponding to recrystallized grains with slightly greater diameters but significantly larger maximum internal misorientation angles. These grains plot along the same trend defined by the porphyroclast data.

4.4. 4.5. Differences between the porphyroclast and neoblast datasets

The porphyroclast and neoblast subsets show significant differences for many descriptive parameters. The grain area distributions for the two datasets have similar shapes, but the area of the neoblasts is nearly two orders of magnitude smaller than the porphyroclasts (Fig. 10, upper panel). Relative to the porphyroclasts, the neoblasts are shaped more equantly (lower aspect ratio) and preserve less internal distortion (lower MIM angles) (Fig. 10).

5. Discussion

5.1. Recrystallization and CPO evolution

Quartz deformed by dislocation processes commonly experiences dynamic recrystallization accommodated by grain boundary migration, subgrain rotation, or both (Urai et al., 1986; Hirth and Tullis, 1992; Stipp et al., 2002a). The influence of these processes on a pre-existing crystallographic fabric are debated (Neumann, 2000; Stipp and Kunze, 2008; Halfpenny et al., 2012), even though a clear understanding of role of recrystallization is essential to the accurate interpretation of CPO. Recrystallized quartz grains often exhibit CPO patterns that can be related to

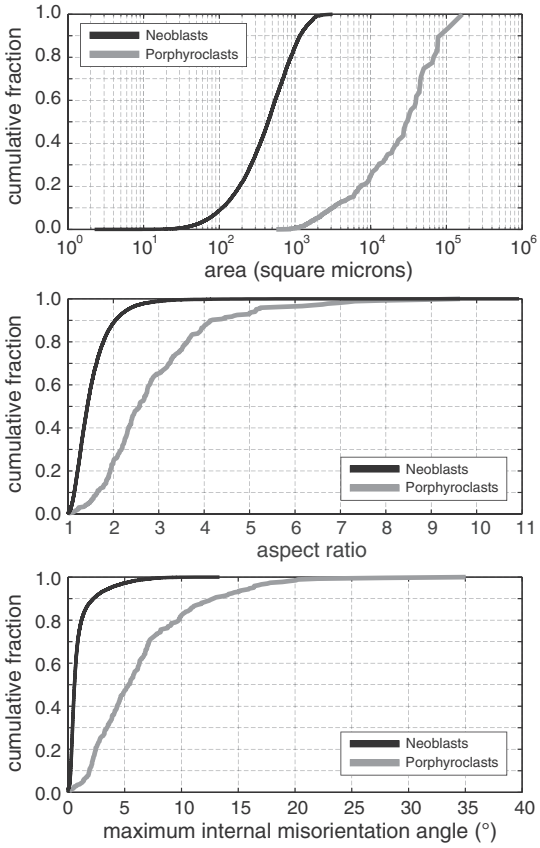

Fig. 10. Cumulative frequency plots for the observed porphyroclast and neoblast distributions, showing grain area (top diagram), aspect ratio (middle), and maximum internal misorientation angle (lower). In comparison to the porphyroclast dataset, the neoblasts are smaller, more equant shaped, and less internally distorted.

slip systems known to be active at particular deformation conditions (Schmid and Casey, 1986; Toy et al., 2008; Morales et al., 2011), and sensible quartz CPOs in recrystallized material have been documented in rocks deformed both experimentally (Hobbs, 1968; Vernooij et al., 2006; Muto et al., 2011) and naturally (e.g., Schmid and Casey, 1986; Stipp et al., 2002b; Law et al., 2010; Keller and Stipp, 2011). For example, Muto et al. (2011) describe deformation experiments performed on single crystals of quartz with varying starting orientations. In their experiments, the recrystallized grains display well-developed and predictable CPO patterns even at relatively low shear values ($\gamma \geq 1$) regardless of original crystal orientation.

The modification of quartz CPO by recrystallization has been demonstrated in experimental and natural examples (Hobbs, 1968; Tullis et al., 1973; Bell and Etheridge, 1976; Neumann, 2000). For example, several studies have documented differences in the quartz CPO in relict and recrystallized grains from the classic mylonitic quartzites from the Stack of Glencoul along the Moine Thrust in Scotland (Law, 1986; Halfpenny et al., 2006; Law et al., 2010). The resulting CPOs are similar, although the recrystallized grains preserve more diffuse patterns and greater quartz opening angles. Halfpenny et al. (2006) argue for an important role for grain boundary sliding (GBS) to explain an observed mixing of recrystallized grains and the weakening of the detrital CPO. In contrast, Law et al. (2010) emphasize that the CPO preserved in the recrystallized material is inconsistent with significant GBS. Instead, they attribute the observed differences in the CPO patterns of the relict versus recrystallized grains to variation in the activity of dislocation glide versus climb in the original versus new grains, possibly due to enhanced hydrolytic weakening for the smaller recrystallized grains.

At first glance, the results of this study could be interpreted similarly. Quartz porphyroclasts, whether analyzed manually or detected from

detailed maps, define a strong cross-girdle CPO characteristic of greenschist-facies deformation (Fig. 5a,b) (Schmid and Casey, 1986). Collectively, the recrystallized grains show a similar fabric (Fig. 5c), albeit with a weaker CPO. The microstructural evidence for dynamic recrystallization and the kinematically-sensible CPO preserved in the recrystallized grains could be readily interpreted as evidence for deformation dominated by the dislocation creep mechanism. Any differences between our porphyroclast and neoblast CPOs could be attributed to slight variations in the contribution of different slip systems.

However, closer inspection suggests that the CPO may record a more complex history of rheological and microstructural evolution. Although in aggregate the neoblasts appear to show a sensible cross-girdle CPO (Fig. 5c), the orientations derived from individual microlithons are generally distinct from the macroscopic fabric. In almost all cases the orientations of recrystallized grains appear to be uniformly dispersed around the orientation of the parent porphyroclast (Fig. 11). It might be argued that continued dislocation creep creates a CPO within the neoblasts like that of the bulk CPO, but in that case we expect that the CPO within each individual microlithon would be similar. Hence, we interpret the neoblast CPO (Fig. 5c) to be inherited rather than derived from ongoing deformation. The neoblasts themselves show little evidence for internal distortion, rarely containing low-angle subgrain boundaries and preserving low MIM angles (Figs. 6 and 8–10). The scarcity of subgrains within neoblasts implies that subgrain rotation recrystallization is only important in the porphyroclasts and does not play a major role in the evolution of the neoblasts CPO. The inverse relationship between fabric intensity and recrystallization fraction for the population of microlithons suggests that progressive strain weakens quartz CPO (Fig. 7). Based on these three observations—(1) the dispersion of neoblasts around the associated porphyroclast orientation, (2) the near-absence of internal deformation, and (3) the progressive weakening of CPO strength with progressive deformation—we infer that dislocation creep is not the predominant deformation mechanism in the recrystallized neoblasts.

Several deformation processes have been proposed to be capable of causing CPO dispersion. For example, cataclasis, twinning, subgrain rotation, and grain boundary sliding associated with diffusion creep may each act to progressively randomize CPO inherited from a parent porphyroclast (see, for example, discussion in Halfpenny et al., 2012). In the case of our sample, some of these processes can be excluded on the basis of microstructural observations. We find no fractures, offset quartz grains, or mineral growth detected during reconnaissance cathodoluminescence analysis that would be indicative of cataclasis as a significant process affecting quartz. Additionally, we discount twinning as a mechanism to reduce CPO strength in our samples; quartz twin laws may increase misorientation angles between grains, but only at discrete values (for example, 60° for Dauphiné twins, or 84.55° for Japan twins) (Menegon et al., 2011; Zhao et al., 2013). The observed

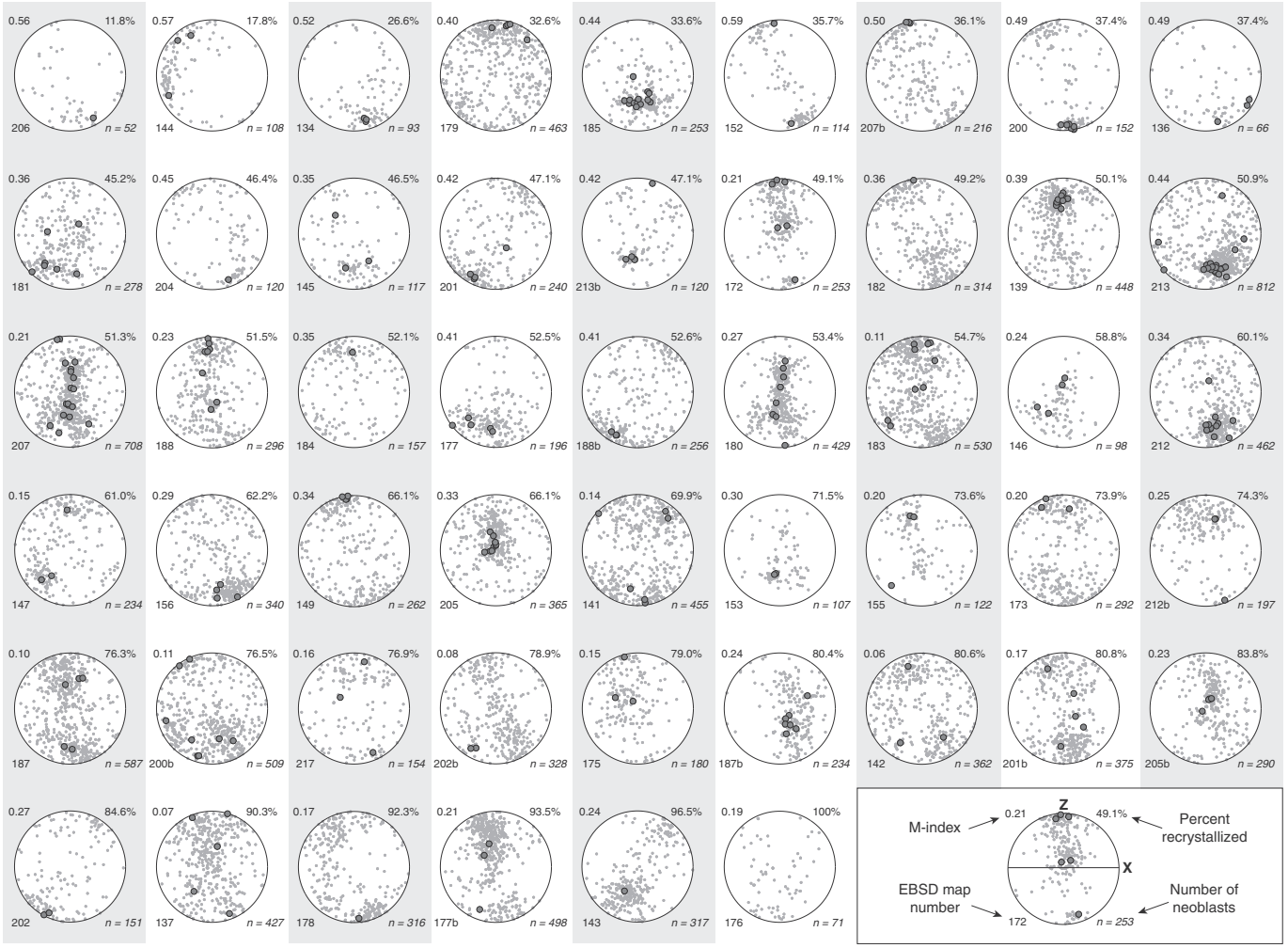

Fig. 11. Lower hemisphere pole figures of quartz c-axes for each of the 51 measured mapped microlithons. Projection plane contains the macroscopic lineation direction (oriented horizontally) and the pole to the foliation plane (oriented vertically). The orientation of individual neoblasts are shown as gray points; the larger dark gray symbols represent the orientations of porphyroclasts (defined as crystals with a grain size at least 4 times the median for a given microlithon). All data represent one point from each grain. The figures are arranged in order of increasing degree of recrystallization.

dispersion of orientations in each mapped microlithon varies smoothly, inconsistent with CPO destruction by the isolated action of twinning.

The process of recrystallization by subgrain rotation itself must also contribute to the destruction of a CPO, given that, by definition, the neoblasts must have a distinct orientation from the relict porphyroclast. Thus, much of the observed dispersion of the neoblasts around the porphyoclasts (Fig. 11) could be explained by the subgrain rotation recrystallization process. Falus et al. (2011) describe similar results from an experimentally deformed mantle xenolith, in which olivine CPO strength decreases with recrystallization due to dispersion associated with subgrain rotation. However, acting in isolation, the subgrain rotation recrystallization process is incapable of generating significant misorientations, as high-angle grain boundaries represent an obstacle to migrating dislocations (Halfpenny et al., 2012). For quartz, this angle is about 10° (White, 1977). Many of the individual microlithons show neoblast orientations dispersed over angular distances well outside of a 10° cone around each porphyoclast, indicating that a process in addition to subgrain rotation recrystallization contributed to fabric dispersion.

We consider diffusion creep and associated GBS as a plausible mechanism for further dispersing neoblast orientations. Grain boundary sliding has been widely invoked as a mechanism for destroying pre-existing CPO in a variety of minerals, quartz (e.g., White, 1979; Law, 1990; Halfpenny et al., 2006; Kilian et al., 2011a), calcite (Bestmann and Prior, 2003), garnet (Bestmann et al., 2008), albite (Jiang et al., 2000), orthopyroxene (Skemer and Karato, 2008), and olivine (Warren and Hirth, 2006). Although unequivocal microstructural evidence for GBS may be difficult to find (Passchier and Trouw, 2005), Halfpenny et al. (2012) summarize features associated with GBS, including smooth and straight grain boundaries, square or rectangular grain shapes, grains arranged parallel to the dominant foliation, and a recrystallized grain size smaller than the dominant subgrain size (White, 1977; White, 1979). In the studied sample, GBS is consistent with microstructural observations of the neoblasts, including their polygonal shapes, straight grain boundaries, and a tendency for grain boundaries to align to form planes parallel to the dominant foliation (Fig. 4).

GBS is thought to enable grains to rotate irrespective of their crystallographic orientation, and therefore tends to produce rocks that lack a strong CPO (Zhang et al., 1994). A finite element model by Wheeler (2009) supports the basic conclusion that GBS can disperse a pre-existing CPO, but also shows that the rate that CPO is dispersed becomes quite slow and that relict fabrics may persist to large strains. Our data are consistent with this interpretation; the decrease of CPO intensity with percent recrystallization may level off at high values of shear strain (Fig. 7). More generally, this analysis suggests a need to consider carefully the common assumption that the CPO of recrystallized material indicates dislocation creep deformation. Collectively, our neoblasts define a sensible CPO, yet individual quartz domains record the progressive dispersion of quartz crystallographic orientations. An important inference is that the CPOs identified in recrystallized materials may be a relict of a pre-recrystallization CPO that is difficult to overprint, even at large strains.

5.2. Rheological evolution

Dynamic recrystallization typically reduces the average grain-size of a polycrystal as porphyroclasts are subdivided into multiple recrystallized grains, the size of which is inversely related to the flow stress (e.g., Stipp and Tullis, 2003). The reduction in grain-size enhances the deformation rate of grain-size sensitive mechanisms such as diffusion creep because the length of the diffusive pathway along grain boundaries is reduced. If diffusion creep is sufficiently enhanced relative to dislocation creep, deformation may undergo a transition in both mechanism and associated rheology (Rutter and Brodie, 1988; Wightman et al., 2006; Kilian et al., 2011a). This transition from grain-size insensitive dislocation creep to grain-size sensitive diffusion creep is associated with a reduction in the flow stress that may contribute to shear localization phenomena, which is a critical factor in the generation of plate tectonics (e.g., Bercovici and Richard, 2012).

As noted above, we infer an important role for diffusion creep and GBS in our sample. To evaluate this possibility, we have constructed a deformation mechanism map to compare microstructural observations to empirical flow laws (Fig. 12). We use the well-established flow laws of Hirth et al. (2001) and Rutter and Brodie (2004) for dislocation creep and diffusion creep, respectively. We estimate deformation temperature with the quartz opening-angle thermometer (Kruhl, 1998; Law, 2014). A fabric skeleton constructed for the quartz porphyroclast CPO pattern exhibits a c-axis opening angle of 40°, suggesting a temperature of about 300 °C (Fig. 5a). However, as emphasized by Law (2014), the thermometer has been calibrated from measurements of recrystallized grains, not relict porphyroclasts like we have sampled; rotations imparted during recrystallization can increase opening angles by as much as 4–20° (Law, 1986; Law, 2014). Adjusting our opening-angle measurement accordingly, the thermometer predicts temperatures from 350 to 450 °C, a range consistent with the observation that feldspars within the ductile deformation zone consistently deform by fracturing (Tullis and Yund, 1987; Bailey et al., 1994). Thus, we regard 400 ± 50 °C as the best estimate for the deformation temperature within the sample. We estimate stress using the Stipp and Tullis (2003) piezometer on the recrystallized grain size; for an average grain size of 32.8 μm (measured through a series of line transects on the thin section and corrected for the stereographic effect), the piezometer predicts a stress of 41.9 MPa (Fig. 12). This result plots well-within the dislocation creep field, such that even large changes in grain-size, temperature, or strain-rate would be insufficient to push the sample into the diffusion creep flow field. Hence, there is an inconsistency between the predictions of the laboratory flow laws and our microstructural interpretations. The flow law determined by Rutter and Brodie (2004) implies that quartz is extremely strong in diffusion creep and unlikely to be important in natural geologic systems, except when temperatures are very high (in excess of 900 K) and grain sizes are extremely small (less than 1 μm). However, our microstructural inferences suggest that diffusion-creep and associated GBS was an active mechanism in the recrystallized material.

Wightman et al. (2006) describe a similar analysis to explain observations from deformed quartz veins in the Alpine Fault of New Zealand. They infer the activity of diffusion creep-accommodated GBS following dislocation creep to explain the destruction of a pre-existing CPO. To reconcile their observations with the known flow laws, Wightman et al. (2006) propose their samples experienced significant grain size reduction (to about 1 μm), a subsequent stress drop that pushed their sample into the diffusion creep field, and a later episode of annealing

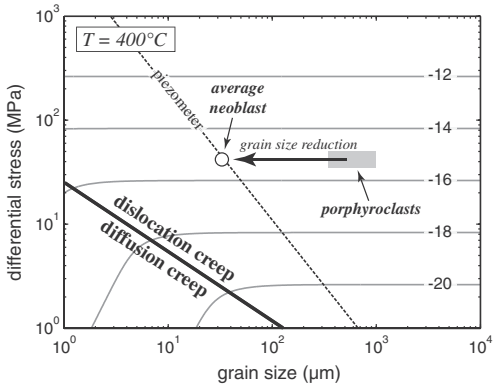

Fig. 12. Deformation mechanism map for quartz, constructed at a temperature of 400 °C using the flow laws of Hirth et al. (2001) for dislocation creep and Rutter and Brodie (2004) for diffusion creep. The dashed black line shows the recrystallized-grain size piezometer of Stipp and Tullis (2003); the open symbol shows the position of our sample. Thin gray lines are strain rate contours in units of s^{-1}.

and grain growth. A complicated scenario like this is necessary to reconcile the observations Wightman et al. (2006) with the proposed flow laws for quartz.

We find no evidence for a significant stress-drop event in our sample, and given the variably deformed and recrystallized nature of the porphyroclasts, it seems likely that stress remained nearly constant throughout the long-term evolution of the rock. Thus, a multi-step model like the one proposed by Wightman et al. (2006) seems inapplicable to our samples. Instead, we favor an alternative possibility, which is that the experimentally-determined diffusion creep flow law does not appropriately capture one or more aspects of deformation under geologic conditions. Rutter and Brodie (2004) acknowledge uncertainty as to how well their quartz diffusion creep flow law can be extrapolated to geologic conditions. One key question is the role of water in enhancing diffusion creep deformation. Farver and Yund (2000) present experimental evidence that silicon diffusion rates are greatly enhanced by the presence of water; their results indicate quartz may deform via diffusion creep for a wide range of grain sizes and metamorphic conditions (Farver and Yund, 2000; Rutter and Brodie, 2004). This phenomenon is better-established for feldspar, for which fluids are known to increase the size of the diffusion creep field on deformation mechanism maps (Tullis and Yund, 1991; Dimanov et al., 1999; Rybacki and Dresen, 2004). In a study of a quartz-rich mylonite from western Japan, Okudairo and Shigematsu (2012) document a transition from dislocation creep to GBS consistent with the flow laws of Hirth et al. (2001) for dislocation creep and Gifkins (1976) for GBS. Notably, their solution incorporates an estimate of water fugacity. Although we lack a quantitative estimate of water in our sample, synkinematic strain fringes of quartz and white mica and fluid inclusions within quartz (Fig. 4) suggest that fluids were present during deformation to enable dissolution-precipitation creep (Rutter, 1983; Urai et al., 1991; Fisher and Brantley, 1992). Our interpretations contribute to a growing body of evidence that grain boundary sliding and diffusion creep, likely assisted by fluid, plays a significant role in natural quartz deformation, despite an apparent conflict with experimentally determined flow laws (Behrmann and Mainprice, 1987; Wightman et al., 2006; Kilian et al., 2011a; Halfpenny et al., 2012; Okudaira and Shigematsu, 2012).

5.3. Implications for rheology of the crust

The partially recrystallized quartz-rich mylonite described here can place constraints on the deformation processes that control the rheology of the mid-crust. The sample captures a transition in microstructure and rheology from a coarse-grained protolith deforming by dislocation creep to a finer-grained rock deforming by diffusion creep and GBS. Due to the limited experimental data on quartz deforming by diffusion creep, the magnitude of weakening cannot be estimated. Nonetheless, we can infer from the rheological transition that some weakening has occurred. As the shear zone accumulated strain, porphyroclasts were progressively replaced by neoblasts. Hence, the fraction of the rock deforming by dislocation creep decreased, and the fraction of the rock deforming by diffusion creep increased. When a critical fraction of recrystallization was achieved, the neoblasts within each microlithon formed an interconnected weak layer (cf., Handy, 1994), leading to a marked reduction in the total strength of the rock. Overall, the systematic relationship between recrystallization fraction, which we interpret to be related to strain, and the evolution of the microstructure, suggests a long transient evolution between rheological steady states.

6. Conclusions

We have documented quartz crystallographic preferred orientations from isolated quartz porphryoclasts in a mid-crustal mylonite. Our study supports the following conclusions:

- Quartz porphyroclasts from a mylonite in the Rockfish Valley Deformation Zone of central Virginia deformed by dislocation creep at temperatures of about 400 ± 50 °C and exhibit variable degrees of recrystallization, spanning a range from nearly unrecrystallized to completely recrystallized.
- Recrystallized grains within a given quartz domain are free of internal distortion and display CPO patterns inconsistent with that of the bulk deformation. Recrystallization occurred by subgrain rotation, which dispersed grain orientations around that of the parent porphyoclast. We infer that continued deformation of these neoblasts occurred by a mechanism capable of further scattering crystallographic orientations, such as grain boundary sliding assisted by fluids.
- Recrystallized quartz grains may preserve a kinematically-sensible CPO. However, such fabrics may be inherited, reflecting the accumulation of CPO during a previous increment of strain history.
- Dynamic recrystallization reduced grain-size that may have triggered a transition to diffusion creep. However, deformation mechanism maps created for the relevant geologic conditions predict that the neoblasts should be deformed by dislocation processes, highlighting the difficulty of extrapolating existing empirical quartz flow laws to naturally-deformed rocks.
- Deformation of the mid-crust is strongly influenced by quartz rheology, and under a wide range of deformation conditions occurs primarily by dislocation creep. However, in settings where deformation is localized, and dynamic recrystallization reduces grain-size sufficiently, rheology may be strongly influenced by grain-size sensitive diffusion creep.

Acknowledgements

Rahl acknowledges generous support from a Lenfest Sabbatical Fellowship and a Lenfest Summer Research Grant from Washington and Lee University. We thank Luiz Morales and David Wallis for thoughtful reviews that helped improve the clarity of the manuscript, and editor Philippe Agard for helpful suggestions. The research is supported in part by NSF EAR—1141795 to Skemer. Karen Roth and Ginny Wala are thanked for assistance in the field and with data acquisition, and Dave Pfaff for photographing the rock slabs.

References

Aleinikoff, J.N., Burton, W.C., Lyttle, P.T., Nelson, A.E., Southworth, C.S., 2000. U–Pb geochronology of zircon and monazite from Mesoproterozoic granitic gneisses of the northern Blue Ridge, Virginia and Maryland, USA. Precambrian Res. 99 (1–2), 113–146.

Bailey, C.M., Simpson, C., 1993. Extensional and contractional deformation in the Blue Ridge Province, Virginia. Geol. Soc. Am. Bull. 105, 411–422.

Bailey, C.M., Simpson, C., De Paor, D.G., 1994. Volume loss and tectonic flattening strain in granitic mylonites from the: Blue Ridge province, central Appalachians. J. Struct. Geol. 16 (10), 1403–1416.

Bartholomew, M.J., Gathright II, T.M., Henika, W.S., 1981. A tectonic model for the Blue Ridge in central Virginia. Am. J. Sci. 281, 1164–1183.

Bartholomew, M.J., Lewis, S.E., Hughes, S.S., Badger, R.L., Sinha, A.K., 1991. Tectonic history of the Blue Ridge basement and its cover, central Virginia. Guidebook [Virginia Museum of Natural History]. 2, pp. 57–90.

Behr, W.M., Platt, J.P., 2011. A naturally constrained stress profile through the middle crust in an extensional terrane. Earth Planet. Sci. Lett. 303 (3), 181–192.

Behrmann, J., Mainprice, D., 1987. Deformation mechanisms in a high-temperature quartz-feldspar mylonite: evidence for superplastic flow in the lower continental crust. Tectonophysics 140 (2), 297–305.

Bell, T., Etheridge, M., 1976. The deformation and recrystallization of quartz in a mylonite zone, central Australia. Tectonophysics 32 (3), 235–267.

Bercovici, D., Richard, Y., 2012. Mechanisms for the generation of plate tectonics by two-phase grain-damage and pinning. Phys. Earth Planet. Inter. 202-203, 27–55.

Bestmann, M., Prior, D.J., 2003. Intragranular dynamic recrystallization in naturally deformed calcite marble: diffusion accommodated grain boundary sliding as a result of subgrain rotation recrystallization. J. Struct. Geol. 25 (10), 1597–1613.

Bestmann, M., Habler, G., Heidelbach, F., Thöni, M., 2008. Dynamic recrystallization of garnet and related diffusion processes. J. Struct. Geol. 30 (6), 777–790.

Botev, Z., Grotowski, J., Kroese, D., 2010. Kernel density estimation via diffusion. Ann. Stat. 38 (5), 2916–2957.

Bürgmann, R., Dresen, G., 2008. Rheology of the lower crust and upper mantle: Evidence from rock mechanics, geodesy, and field observations. Annu. Rev. Earth Planet. Sci. 36 (1), 531.
Campbell, P.A., Anderson, T.H., 1992. Kinematic analysis of a mylonite zone between the Pedlar and Lovingston Massifs in central Virginia. The Compass: Earth Science Journal of Sigma Gamma Epsilon 69, 257–271.
Carreras, J., García Celma, A., 1982. Quartz of C-axis fabric variation at the margins of a shear zone developed in shists from cap de Creus (Spain). Acta Geol. Hisp. 17 (3), 137–149.
Dimanov, A., Dresen, G., Xiao, X., Wirth, R., 1999. Grain boundary diffusion creep of synthetic anorthite aggregates: the effect of water. J. Geophys. Res. Solid Earth 104 (B5), 10483–10497 (1978–2012).
Evans, N.H., 1991. Latest Precambrian to Ordovician metamorphism in the Virginia Blue Ridge: origin of the contrasting Lovingston and Pedlar basement terranes. Am. J. Sci. 291, 425–452.
Falus, G., Tommasi, A., Soustelle, V., 2011. The effect of dynamic recrystallization on olivine crystal preferred orientations in mantle xenoliths deformed under varied stress conditions. J. Struct. Geol. 33 (11), 1528–1540.
Farver, J., Yund, R., 2000. Silicon diffusion in a natural quartz aggregate: constraints on solution-transfer diffusion creep. Tectonophysics 325 (3), 193–205.
Fisher, D.M., Brantley, S.L., 1992. Models of quartz overgrowth and vein formation: deformation and episodic fluid flow in an ancient subduction zone. J. Geophys. Res. 97 (B13), 20043–20061.
Gifkins, R., 1976. Grain-boundary sliding and its accommodation during creep and superplasticity. Metall. Trans. A 7 (8), 1225–1232.
Halfpenny, A., Prior, D.J., Wheeler, J., 2006. Analysis of dynamic recrystallization and nucleation in a quartzite mylonite. Tectonophysics 427 (1), 3–14.
Halfpenny, A., Prior, D.J., Wheeler, J., 2012. Electron backscatter diffraction analysis to determine the mechanisms that operated during dynamic recrystallisation of quartz-rich rocks. J. Struct. Geol. 36, 2–15.
Handy, M.R., 1994. Flow laws for rocks containing two non-linear viscous phases; a phenomenological approach. J. Struct. Geol. 16 (3), 287–301.
Heilbronner, R., Tullis, J., 2002. The effect of static annealing on microstructures and crystallographic preferred orientations of quartzites experimentally deformed in axial compression and shear. Geol. Soc. Lond. Spec. Publ. 200 (1), 191–218.
Heilbronner, R., Tullis, J., 2006. Evolution of c axis pole figures and grain size during dynamic recrystallization: results from experimentally sheared quartzite. J. Geophys. Res. 111 (B10), B10202.
Hielscher, R., Schaeben, H., 2008. A novel pole figure inversion method: specification of the MTEX algorithm. J. Appl. Crystallogr. 41 (6), 1024–1037.
Hirth, G., Tullis, J., 1992. Dislocation creep regimes in quartz aggregates. J. Struct. Geol. 14 (2), 145–159.
Hirth, G., Teyssier, C., Dunlap, W.J., 2001. An evaluation of quartzite flow laws based on comparisons between experimentally and naturally deformed rocks. Int. J. Earth Sci. 90, 77–87.
Hobbs, B., 1968. Recrystallization of single crystals of quartz. Tectonophysics 6 (5), 353–401.
Hull, J., 1988. Thickness-displacement relationships for deformation zones. J. Struct. Geol. 10 (4), 432–435.
Jenkins, C., Bailey, C.M., Kunk, M.J., 2012. Argon thermochronology in the central Virginia Blue Ridge and Piedmont. Proceedings Geological Society of America Abstracts with Programs. 44, p. 73.
Jiang, Z., Prior, D.J., Wheeler, J., 2000. Albite crystallographic preferred orientation and grain misorientation distribution in a low-grade mylonite: implications for granular flow. J. Struct. Geol. 22, 1663–1674.
Kaczmarek, M.A., Tommasi, A., 2011. Anatomy of an extensional shear zone in the mantle, Lanzo massif, Italy. Geochem. Geophys. Geosyst. 12 (8).
Keller, L.M., Stipp, M., 2011. The single-slip hypothesis revisited; crystal-preferred orientations of sheared quartz aggregates with increasing strain in nature and numerical simulation. J. Struct. Geol. 33 (10), 1491–1500.
Kilian, R., Heilbronner, R., Stünitz, H., 2011a. Quartz grain size reduction in a granitoid rock and the transition from dislocation to diffusion creep. J. Struct. Geol. 33 (8), 1265–1284.
Kilian, R., Heilbronner, R., Stünitz, H., 2011b. Quartz microstructures and crystallographic preferred orientation: which shear sense do they indicate? J. Struct. Geol. 33 (10), 1446–1466.
Knoll, M., Tommasi, A., Logé, R.E., Signorelli, J.W., 2009. A multiscale approach to model the anisotropic deformation of lithospheric plates. Geochem. Geophys. Geosyst. 10 (8).
Kocks, U.F., Tomé, C.N., Wenk, H.-R., 2000. Texture and Anisotropy: Preferred Orientations in Polycrystals and Their Effect on Materials Properties. Cambridge University Press.
Kohlstedt, D., Evans, B., Mackwell, S., 1995. Strength of the lithosphere: constraints imposed by laboratory experiments. J. Geophys. Res. Solid Earth 100 (B9), 17587–17602 (1978–2012).
Kruhl, J., 1998. Reply: prism-and basal-plane parallel subgrain boundaries in quartz: a microstructural geothermabarometer. Journal of Metamorphic Petrology 16.
Law, R.D., 1986. Relationships between strain and quartz crystallographic fabrics in the Roche Maurice quartzites of Plougastel, western Brittany. J. Struct. Geol. 8, 493–516.
Law, R.D., 1990. Crystallographic fabrics: a selective review of their applications to research in structural geology. In: Knipe, R.J., Rutter, E.H. (Eds.), Deformation Mechanism, Rheology and Tectonics. Geological Society Special Publication No. 54, pp. 335–352.
Law, R.D., 2014. Deformation thermometry based on quartz c-axis fabrics and recrystallization microstructures: a review. J. Struct. Geol. 66, 129–161.
Law, R.D., Mainprice, D., Casey, M., Lloyd, G.E., Knipe, R., Cook, B., Thigpen, J., 2010. Moine thrust zone mylonites at the stack of Glencoul: I—microstructures, strain and influence of recrystallization on quartz crystal fabric development. Geol. Soc. Lond. Spec. Publ. 335 (1), 543–577.
Linckens, J., Herwegh, M., Muentener, O., Mercolli, I., 2011. Evolution of a polymineralic mantle shear zone and the role of second phases in the localization of deformation. J. Geophys. Res. Solid Earth 116.
Lister, G., 1977. Discussion: crossed-girdle c-axis fabrics in quartzites plastically deformed by plane strain and progressive simple shear. Tectonophysics 39 (1), 51–54.
Lloyd, G.E., Farmer, A.B., Mainprice, D., 1997. Misorientation analysis and the formation and orientation of subgrain and grain boundaries. Tectonophysics 279 (1), 55–78.
Mehl, L., Hirth, G., 2008. Plagioclase preferred orientation in layered mylonites: evaluation of flow laws for the lower crust. J. Geophys. Res. Solid Earth 113 (B5) (1978–2012).
Menegon, L., Piazolo, S., Pennacchioni, G., 2011. The effect of Dauphiné twinning on plastic strain in quartz. Contrib. Mineral. Petrol. 161 (4), 635–652.
Morales, L.F., Mainprice, D., Lloyd, G.E., Law, R.D., 2011. Crystal fabric development and slip systems in a quartz mylonite: an approach via transmission electron microscopy and viscoplastic self-consistent modelling. Geol. Soc. Lond. Spec. Publ. 360 (1), 151–174.
Muto, J., Hirth, G., Heilbronner, R., Tullis, J., 2011. Plastic anisotropy and fabric evolution in sheared and recrystallized quartz single crystals. J. Geophys. Res. 116 (B2), B02206.
Neumann, B., 2000. Texture development of recrystallised quartz polycrystals unravelled by orientation and misorientation characteristics. J. Struct. Geol. 22 (11), 1695–1711.
Okudaira, T., Shigematsu, N., 2012. Estimates of stress and strain rate in mylonites based on the boundary between the fields of grain-size sensitive and insensitive creep. J. Geophys. Res. Solid Earth 117 (B3) 1978–2012.
Passchier, C.W., Trouw, R.A.J., 2005. Microtectonics. Springer, Berlin (366 p).
Précigout, J., Gueydan, F., Gapais, D., Garrido, C., Essaifi, A., 2007. Strain localisation in the subcontinental mantle—a ductile alternative to the brittle mantle. Tectonophysics 445 (3), 318–336.
Rader, E., Evans, N., 1993. Geologic Map of Virginia—Expanded Explanation: Virginia Division of Mineral Resources.
Raimbourg, H., Toyoshima, T., Harima, Y., Kimura, G., 2008. Grain-size reduction mechanisms and rheological consequences in high-temperature gabbro mylonites of Hidaka, Japan. Earth Planet. Sci. Lett. 267 (3), 637–653.
Randle, V., Engler, O., 2000. Introduction to Texture Analysis: Macrotexture, Microtexture and Orientation Mapping. CRC Press.
Rutter, E.H., 1983. Pressure solution in nature, theory and experiment. J. Geol. Soc. Lond. 140, 725–740.
Rutter, E., Brodie, K., 1988. The role of tectonic grain size reduction in the rheological stratification of the lithosphere. Geol. Rundsch. 77 (1), 295–307.
Rutter, E.H., Brodie, K.H., 2004. Experimental grain size-sensitive flow of hot-pressed Brazilian quartz aggregates. J. Struct. Geol. 26 (11), 2011–2023.
Rybacki, E., Dresen, G., 2004. Deformation mechanism maps for feldspar rocks. Tectonophysics 382 (3), 173–187.
Schmid, S.M., Casey, M., 1986. Complete fabric analysis of some commonly observed quartz c-axis patterns. In: Hobbs, B.E., Heard, H.C. (Eds.), Mineral and Rock Deformation. Laboratory Studies (The Paterson Volume), pp. 263–268.
Sinha, A.K., Bartholomew, M.J., 1984. Evolution of the Grenville terrane in the central Virginia Appalachians. Geol. Soc. Am. Spec. Pap. 194, 175–186.
Skemer, P., Karato, S., 2008. Sheared lherzolite xenoliths revisited. J. Geophys. Res. 113, B07205.
Skemer, P., Katayama, I., Jiang, Z., Karato, S., 2005. The misorientation index: development of a new method for calculating the strength of lattice-preferred orientation. Tectonophysics 411 (1), 157–167.
Skemer, P., Warren, J.M., Hansen, L.N., Hirth, G., Kelemen, P.B., 2013. The influence of water and LPO on the initiation and evolution of mantle shear zones. Earth Planet. Sci. Lett. 375, 222–233.
Spencer, E.W., 1995. Intersection of the Blue Ridge Fault with ductile deformation zones in the Blue Ridge basement. Southeast. Geol. 35 (3), 123–138.
Stipp, M., Kunze, K., 2008. Dynamic recrystallization near the brittle-plastic transition in naturally and experimentally deformed quartz aggregates. Tectonophysics 448 (1–4), 77–97.
Stipp, M., Tullis, J., 2003. The recrystallized grain size piezometer for quartz. Geophys. Res. Lett. 30 (21).
Stipp, M., Stünitz, H., Heilbronner, R., Schmid, S.M., 2002a. Dynamic recrystallization of quartz; correlation between natural and experimental conditions. Geol. Soc. Spec. Publ. 200, 171–190.
Stipp, M., Stünitz, H., Heilbronner, R., Schmid, S.M., 2002b. The eastern Tonale fault zone; a 'natural laboratory' for crystal plastic deformation of quartz over a temperature range from 250 to 700 degrees C. J. Struct. Geol. 24 (12), 1861–1884.
Toy, V.G., Prior, D.J., Norris, R.J., 2008. Quartz fabrics in the Alpine Fault mylonites: influence of pre-existing preferred orientations on fabric development during progressive uplift. J. Struct. Geol. 30 (5), 602–621.
Toy, V.G., Prior, D.J., Norris, R.J., Cooper, A.F., Walrond, M., 2012. Relationships between kinematic indicators and strain during syn-deformational exhumation of an oblique slip, transpressive, plate boundary shear zone: the Alpine Fault, New Zealand. Earth Planet. Sci. Lett. 333, 282–292.
Tullis, J., Yund, R.A., 1987. Transition from cataclastic flow to dislocation creep of feldspar: mechanisms and microstructures. Geology 15 (7), 606–609.
Tullis, J., Yund, R.A., 1991. Diffusion creep in feldspar aggregates: experimental evidence. J. Struct. Geol. 13 (9), 987–1000.
Tullis, J.T., et al., 1973. Microstructures and preferred orientations of experimentally deformed quartzites. Geol. Soc. Am. Bull. 84, 297–314.
Urai, J., Means, W., Lister, G., 1986. Dynamic recrystallization of minerals. Geophysical Monograph Series 36, 161–199.
Urai, J.L., Williams, P.F., van Roermund, H.L.M., 1991. Kinematics of crystal growth in syntectonic fibrous veins. J. Struct. Geol. 13 (7), 823–836.

Vernooij, M.G., den Brok, B., Kunze, K., 2006. Development of crystallographic preferred orientations by nucleation and growth of new grains in experimentally deformed quartz single crystals. Tectonophysics 427 (1), 35–53.
Warren, J.M., Hirth, G., 2006. Grain size sensitive deformation mechanisms in naturally deformed peridotites. Earth Planet. Sci. Lett. 248, 438–450.
Wheeler, J., 2009. The preservation of seismic anisotropy in the Earth's mantle during diffusion creep. Geophys. J. Int. 178 (3), 1723–1732.
Wheeler, J., Mariani, E., Piazolo, S., Prior, D.J., Trimby, P., Drury, M., 2012. The weighted burgers vector: a quantity for constraining dislocation densities and types using electron backscatter diffraction on 2D sections through crystalline materials. Proceedings Materials Science Forum 715. Trans Tech Publ, pp. 732–736.
White, S., 1976. The effects of strain on the microstructures, fabrics, and deformation mechanisms in quartzites: philosophical transactions of the Royal Society of London. Proc. R. Soc. Lond. A Math. Phys. Sci. 283 (1312), 69–86.
White, S.H., 1977. Geological significance of recovery and recrystallization processes in quartz. Tectonophysics 39, 143–170.
White, S., 1979. Grain and sub-grain size variations across a mylonite zone. Contrib. Mineral. Petrol. 70 (2), 193–202.
Wightman, R.H., Prior, D.J., Little, T.A., 2006. Quartz veins deformed by diffusion creep-accommodated grain boundary sliding during a transient, high strain-rate event in the Southern Alps, New Zealand. J. Struct. Geol. 28 (5), 902–918.
Zhang, Y., Hobbs, B., Jessell, M., 1994. The effect of grain-boundary sliding on fabric development in polycrystalline aggregates. J. Struct. Geol. 16 (9), 1315–1325.
Zhao, S.-R., Xu, H.-J., Wang, Q.-Y., Yang, K.-G., 2013. Electron backscatter diffraction study of twins and intergrowths among quartz crystals in granite. J. Appl. Crystallogr. 46 (5), 1414–1424.